frontiers in Marine Science

Climate change will fragment Florida stone crab communities

Lauranne Alaerts[1,2*], Thomas Dobbelaere[1], Philip M. Gravinese[3] and Emmanuel Hanert[1,4]

[1] Earth and Life Institute, UCLouvain, Louvain-la-Neuve, Belgium
[2] MAST, FOCUS, University of Liège, Liège, Belgium
[3] Department of Biological Sciences, Florida Southern College, Lakeland, FL, 33801, USA
[4] Institute of Mechanics, Materials and Civil Engineering, UCLouvain, Louvain-la-Neuve, Belgium

*** Correspondence:** Corresponding Author: lauranne.alaerts@uclouvain.be

Keywords: climate change, population connectivity, stone crab, Florida, multi-scale biophysical modeling.

Abstract

The tolerance of many marine species is being threatened by both ocean acidification and ocean warming which are reducing survival, altering behavior, and posing limits on physiology, especially during earlier life stages. The commercially important Florida stone crab, *Menippe mercenaria*, is one species that is affected by changes in seawater pH and temperature. In this study, we determined the impacts of reduced pH and elevated temperature on the distribution of the stone crab larvae along the West Florida Shelf. To understand the dispersion of the larvae, we coupled the multi-scale ocean model SLIM with a larval dispersal model. We then conducted a connectivity study and evaluated the impacts of climate change by looking at three different scenarios which included models that represented the dispersion of stone crab larvae under: 1) present day conditions (pH = 8.0), 2) moderate pH (-0.275 reduction in pH) and temperature changes (+ 1 °C), and 3) extreme pH (-0.43 reduction in pH) and temperature conditions (+3 °C). Our results show a clear impact of these climate change stressors on larval dispersal and on the subsequent stone crab distribution. Future climate change could result in stone crabs moving north or into deeper waters. We also observed an increase in the number of larvae settling in deeper waters (defined as the non-fishing zone in this study with depths exceeding 30 m) that are not typically part of the commercial fishing zone. The distance travelled by larvae, however, is likely to decrease, resulting in an increase of self-recruitment and decrease of the size of the sub-populations. Our results suggest that habitats in the non-fishing zone cannot serve as a significant source of larvae for the habitats in the fishing zone (defined as water depth < 30 m) since there is very little exchange (< 5% of all exchanges) between the two zones. These results indicate that the stone crab populations in Florida may be susceptible to community fragmentation and that the management of the fishery should consider the potential impacts of future climate change scenarios.

1 Introduction

Anthropogenic inputs, like excess atmospheric CO_2, is resulting in a warmer, more acidic ocean. At the current rate, the ocean's temperature could increase by 1-3°C by 2100, while the pH could decrease by 0.14-0.43 unit (Hoegh-Guldberg et al., 2014; Fox-Kemper et al., 2021). These global effects are compounded by localized inputs in many coastal habitats, such as increasing organic nutrient loads into coastal zones, that further increase CO_2 concentration and hence reduce pH. Coastal areas are also more threatened by the increase in seawater temperature as they warm faster than open ocean

(Hoegh-Guldberg et al., 2014; Fox-Kemper et al., 2021). In addition, reductions in seawater pH and increases in seawater temperature can have deleterious effects on many coastal species, especially during earlier life-stages, which are often more sensitive than adult conspecifics (Kurihara, 2008; Ceballos-Osuna et al., 2013; Bednaršek et al., 2021). Crustaceans are especially sensitive to those changes. Higher temperatures can lead to an acceleration in their metabolism and destabilize the proteins (Young and Hazlett, 1978). For some species, exposure to combined stressors of reduced pH and elevated temperature can lead to shorter larval stages, a higher mortality rate and smaller individuals (Kuhn, 2017). Additionally, synergistic effects between acidification and warmer water have been observed for several crustacean species, resulting in high mortality, hypercapnia and reduction in oxygen circulation (Metzger et al., 2007; Dissanayake and Ishimatsu, 2011; Gravinese et al., 2018).

The stone crab (*Menippe mercenaria*) is an economically important species in Florida, where its commercial value is about $25-30 million annually (Florida Fish and Wildlife Conservation Commission 1998-2018). The landings (i.e. only the claws) peaked in the 2000-01 fishing season with a total of 3.5 million pounds of claws statewide and has since declined by ~30% (Muller et al., 2011). Recent studies have shown that the stone crab is sensitive to rising ocean temperature and acidification (Gravinese, 2018; Gravinese et al., 2018, 2019). Elevated temperature significantly reduces larval survivorship (Brown et al., 1992; Gravinese et al., 2018), while reductions in seawater pH have been shown to slow embryonic development rate (and hence increase the time to hatching), reduce hatching success (Gravinese, 2018) and change the larval vertical swimming behavior (Gravinese et al., 2019). Like all brachyuran crabs, *M. mercenaria* has a complex life cycle, made of four main stages: the larval stage, which is composed of five zoeal stages, the post-larval or megalopal stage, the juvenile stage and the adult stage (Sulkin, 1984; Gulf Shores Marine Fisheries Commission, 2001). Each zoeal stage lasts between about 3 to 6 days (Porter, 1960), but these durations can drastically change with temperature (Brown et al., 1992). Stone crab larvae require warm water and high salinity, with the highest survival rate observed in laboratory studies at 30°C and around 30-35 ppt respectively (Porter, 1960; Lindberg and Marshall, 1984; Brown et al., 1992). Stone crab larvae also have vertical swimming behaviors in response to changes in light and hydrostatic pressure. For example, stage 1 and 3 larvae exhibit negative geotaxis, hence positioning themselves at shallower depths. This is however counterbalanced by a negative phototactic response that makes them migrate deeper in the water column during the day and then return near to the surface at night (Gravinese, 2018). The sensitivity to gravity, light, and pressure changes in stage 5 larvae, which exhibit a positive geotaxis resulting in positioning deeper in the water column to more easily find settlement habitats. All larval stages exhibit an upward (downward) movement when exposed to increasing (decreasing) hydrostatic pressure (Gravinese, 2018).

The defined larval vertical swimming behaviors provide a feedback mechanism for regulating their relative depth distribution (Gravinese, 2018). Understanding the vertical swimming behavior of stone crab larvae can help describe the dispersion, recruitment patterns, and the larval exchanges between the different stone crab habitats, which could help to further improve the sustainable management of the stone crab fishery. This can be done through biophysical modeling and genetic studies (Pineda et al., 2007; Baeza et al., 2019; Seyoum et al., 2021). While genetic studies can identify if genetical material has been exchanged between habitats, they cannot provide the timing and the importance of those exchanges (Cowen and Sponaugle, 2009). Biophysical dispersal models can provide a more accurate picture of larval dispersal and exchanges between separated habitats over temporal scales. Such an approach has been used to model other brachyuran crabs dispersion, such as the European green crab (*Carcinus maenas*) and the blue crab (*Callinectes sapidus*) (Peliz et al., 2007; Banas et al., 2009; Criales et al., 2019).

Here, we used a multi-scale biophysical model to evaluate the potential impacts of climate change on the dispersion of the stone crab larvae along the West Florida Shelf (WFS). We used the 3D version of the Second-generation Louvain-la-Neuve Ice-Ocean Model[1] to simulate the hydrodynamics over the WFS and couple it with a larval dispersal model that represents the biological swimming traits of the different stages of stone crab larvae. Our objective was to (1) assess how stone crab larval dispersal and connectivity will be modified under different climate change scenarios (i.e., reduced pH and elevated temperature) and (2) estimate the potential for non-fishing areas (defined as depths > 30m, (Muller et al., 2011)) to repopulate habitats that occur in the predominate fishing areas (defined as depths < 30 m).

2 Data and methods

2.0 Stone crab habitats

The predominate stone crab fishery occurs along the WFS which is in the eastern part of the Gulf of Mexico (GOM), and stretches from Apalachicola Bay to the Florida Keys (FK). The WFS is a broad continental shelf, reaching about 250 km offshore and has a maximum depth of about 110 m (**Figure 1a**). The circulation on the WFS is mainly driven by local winds but is also forced by tides, buoyancy fluxes and by the Loop Current (Weisberg et al., 2001). The WFS is also subject to seasonal changes in circulation. The circulation is predominantly downwelling-favorable during summer months and upwelling-favorable during the winter months. The amplitude and direction of the horizontal currents also present a seasonal dynamic due to the seasonal wind variability. On the inner shelf, where the bathymetry is shallower, the monthly mean current amplitude ranges from 2-12 cm/s from fall to spring and decreases to 0-6cm/s during summer months. The direction of the currents tends to be southeastward between October and April, and northwestward between June and September. The seasonal variability is less pronounced below 50m depth (Liu and Weisberg, 2012). On the outer shelf, seasonal variations are drowned out by the influence of water circulation from the rest of the Gulf. In our study, the hydrodynamic model outputs were validated with respect to velocity and temperature observations from the NOAA stations 42013 (27.173°N, 82.924°W), 42022 (27.505°N, 83.741°W) and 42023 (26.010° N, 83.086° W). Station locations are shown in **Figure 1a**.

Since there are no stone crab habitat maps for the WFS, we used a seafloor substrate map and assumed that all rocky, muddy or gravely substrates shallower than 60 m could be suitable stone crab habitats (Bert et al., 1978; Beck, 1995; Krimsky and Epifanio, 2008). A seafloor substrate map was made by the Institute of Arctic and Alpine research of the University of California and has a resolution of 4km^2 (INSTAAR, 2011). The selection of benthic habitats was validated by looking at punctual observations reported on the Global Biodiversity Information Facility (GBIF) between 2011 and 2021 (GBIF Backbone Taxonomy, 2019). As a result, our study considered 3858 habitat patches of 4 km^2 (**Figure 1b**). Among these habitats, we further distinguish between habitats that are fished vs. habitats that are normally not fished (hereon characterized as non-fishing habitats). The former corresponds to habitats shallower than 30 m as we assumed that fishing is not economically viable at greater depths (Muller et al., 2011). There is therefore a clear separation between fishing and non-fishing habitats, which corresponds to the 30m isobath (**Figure 1b**).

[1] SLIM, https://www.slim-ocean.be/

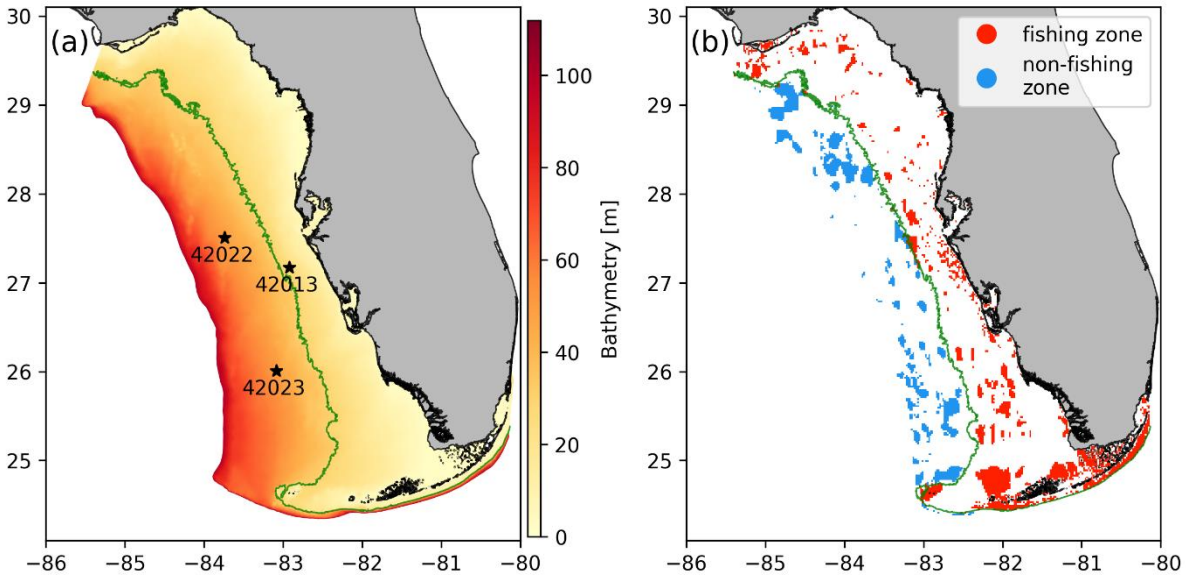

Figure 1 : *Model computational domain with **(a)** the bathymetry and location of validation stations for the hydrodynamics (black stars) and **(b)** the stone crabs' habitats and their distribution between fishing and non-fishing zone. The green line represents the 30m isobath that separates the fishing and non-fishing zones.*

2.1 Habitat connectivity model

Hydrodynamic model

We simulate the three-dimensional ocean circulation over the WFS with the multi-scale ocean model SLIM. SLIM solves the 3D hydrostatic governing equations under the Boussinesq approximation (Vallaeys et al., 2018, 2021; Duquesne et al., 2021). The model equations are discretized with the discontinuous Galerkin finite element method on a 3D mesh made of triangular prisms. The 3D mesh is obtained by extruding an unstructured 2D mesh made of triangles in the vertical. The horizontal resolution can be locally increased to better represent small-scale circulation features driven by the topography or by the bathymetry. The horizontal mesh resolution depends on the distance to the coast, the distance to stone crabs' habitats, the bathymetry and the bathymetry gradient. The horizontal resolution reaches 400 m along the coast and about 10 km offshore (**Figure 2a**). The vertical dimension is discretized with 20 terrain-following sigma layers that are clustered near the surface such that there are at least 5 layers in the top 11 meters.

The model bathymetry is extracted from the Coastal Relief Model, which offers a representation of the US coast with a resolution of 3 arc-seconds, or roughly 90 m (NOAA National Geophysical Data Center, 2001). The model dynamics are forced on the boundaries by wind, tides, surface heat and salinity fluxes and the large-scale circulation from the GOM. The resulting circulation correctly reproduces the large-scale flow features over the WFS as well as smaller-scale flow features driven by the topography (**Figure 2b**). We provide additional details on the model formulation and its validation with respect to NOAA stations data in the Supplementary Materials.

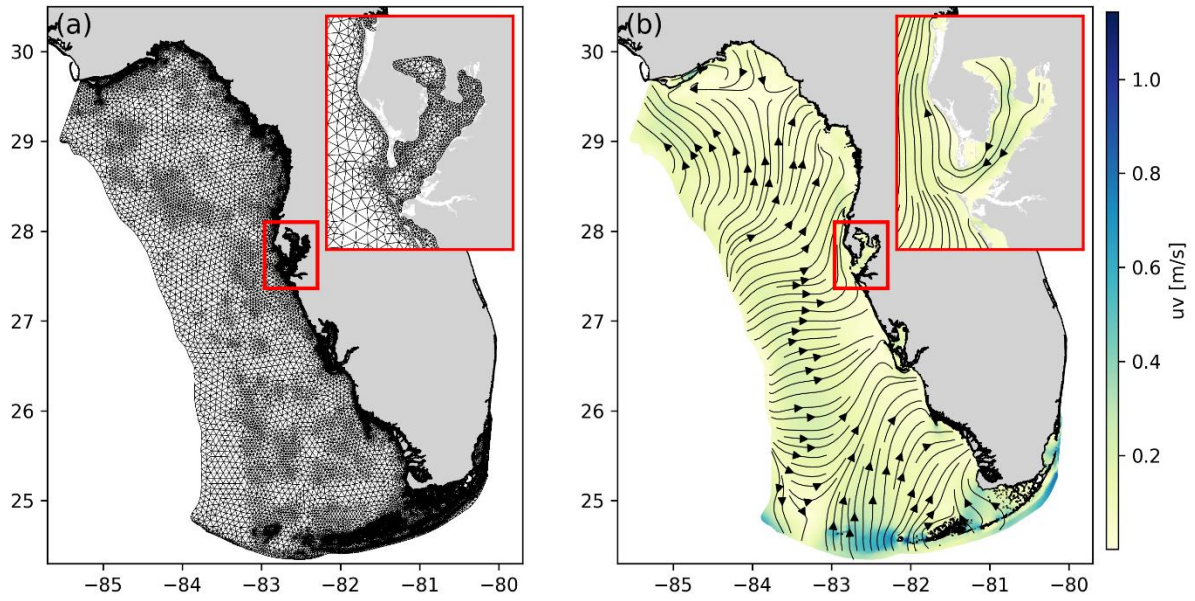

***Figure 2** : Model computational domain with a close-up view on Tampa Bay showing **(a)** the horizontal unstructured mesh whose resolution ranges between 400m and 10km and **(b)** a snapshot of the surface circulation as modelled by SLIM on the 15th of July, 2019 at 00:00, with uv as the horizontal water speed.*

Larval transport model

The simulated currents are then used to model the transport of virtual crab larvae by using a Lagrangian biophysical model. The model simulates larval dispersal following 7 spawning events, separated by 21 days and starting on May 1st, 2019, at 14:00. Each spawning event lasts for 20 hours, with a release rate of 1 particle per km^2 and per hour. Each particle represents a large number of real larvae and is characterized by an initial mass that exponentially decreases with time to represent larval mortality. Larvae are released 1 m above the stone crabs' habitats. The larval advection velocity is the sum of the currents' 3D velocity and the larval vertical swimming velocity. Larval advection velocity is integrated with a 4th order Runge-Kutta scheme. The model also includes a stochastic diffusion term represented as a Wiener process with a diffusivity calculated using Okubo (1971)'s formula.

Biological processes representing larval life history traits include the duration of each larval stage, the survival rate and the vertical swimming behaviour. The duration of each larval stage varies according to temperature as observed by Brown et al. (1992). We used their data for larvae that hatched from eggs developed at sea to build a general multivariate regression model that gives the duration of each larval stage as a function of temperature. The resulting regression has an adjusted R^2 value of 0.95 and the F-test gave a significant result ($F = 64.16$; $P < 0.0001$). We used the temperature at the beginning of each larval stage to determine the duration of that stage. The survival rate for each larval stage is based on observations from Brown et al. (1992) and Gravinese et al. (2018). We derived equations describing the survival rate of each stage, according to temperature (and salinity for the first larval stage) by using a general linear model. The proportion of surviving larvae is calculated at the end of each stage.

We modeled the larval vertical swimming behaviors according to their known responses to light, hydrostatic pressure and pH as measured by Gravinese (2018), Gravinese et al. (2018) and Gravinese et al., (2019). Since the different stages react differently to those external factors, we defined the vertical velocity of each stage separately. Larvae's response to light was defined by using the time of

the day. Larval stages 1 to 3 were characterized with an upward swimming behaviour during the night (between 18:00 and 06:00) and a downward swimming behaviour during the day (between 06:00 and 18:00). Similar approaches have been used in other studies that take daily migration of crabs' larvae into account (Peliz et al., 2007; Banas et al., 2009; Pires et al., 2020). However, unlike those studies, we chose not to have fixed velocities during the day/night, but instead used a smooth sinusoidal function for larval velocity with a period of 24 hours. Our model assumes that larval stages 4 and 5 are less sensitive to light resulting in constant downward vertical velocities. The vertical velocity in response to pH was defined based on observation made by Gravinese et al. (2019). They observed that stage 3 larvae swimming behaviour reverses with reduced seawater pH, while swimming behaviour of stage 5 larvae was unaffected (i.e., still a downward response). We therefore impose an identical pH-dependent vertical velocity for stages 1 to 3, and a vertical velocity that does not depend on pH for stages 4 and 5.

Finally, all larval stages respond to changes in pressure. According to (Gravinese, 2018), at a rate of 0.1 mbar/sec, stages 1, 3 and 5 react to a pressure increase of 80 mbar, 60 mbar and 100 mbar, respectively. At the same rate, stages 1 and 3 react to a 60 mbar and 100 mbar decrease, respectively. That pressure effect results in a decrease of the vertical velocity of the larvae. We have therefore represented the effect of changes in hydrostatic pressure by multiplying the larval vertical velocity by a stage-dependent damping factor.

Larvae become sensitive to cues from suitable settlement habitats in their final development stage, called the megalopal stage. No information was available concerning the vertical velocity of this stage. We therefore defined its vertical velocity as being equal to the reported mean downward swimming velocity of stage-5 larvae Gravinese (2018). The duration of this stage is set to 13 days, as this was the longest duration observed for this stage by Brown et al. (1992). If the megalopa finds itself one meter or less above a habitat during that time, it will settle down on that habitat. If the megalopa has not settled on any suitable habitat after 13 days, it dies and is removed of the simulation. More details on the larval transport model formulation are provided in the supplementary materials.

2.2 Connectivity indicators

The larval transport model yields a potential connectivity matrix C_{ij} whose entries correspond to the number of virtual larvae produced on habitat *i* that settled on habitat *j*. Since we consider 3858 separated crab habitats, the connectivity matrix has ~1.5×10^7 entries. The connectivity matrix is usually normalized by dividing all the entries of a given row by the number of larvae seeded on the corresponding source reef. The resulting matrix $\tilde{C}_{ij}$ then represents the probability of connection between habitats. While most of the connectivity matrix entries are empty, it remains challenging to analyse such a large matrix. One way to make the task easier is to interpret the connectivity matrix as a large graph whose nodes are the crab habitats, and the edges correspond to the non-zero entries in the connectivity matrix. The strength of an edge directed from node *i* to node *j* simply corresponds to $\tilde{C}_{ij}$.

Many graph-theory indicators are available to extract useful information from the connectivity graph (see for instance Minor and Urban, 2007; Rayfield et al., 2011; Kool et al., 2013; Dubois et al., 2016). Here, we only consider indicators that best highlight the connectivity differences resulting from climate change. First, we consider a source index that identifies habitats that export many larvae to many different habitats. This can be obtained by combining the habitat out-degree (i.e. the number of outgoing connections) and the number of larvae exported from that habitat to other habitats:

$$SI_i = N_i^{out} \cdot \sum_j \tilde{C}_{ij},$$

where N_i^{out} is the out-degree of habitat *i*. We also consider self-recruitment, which identifies isolated habitats by looking at the fraction of settlers that were locally produced:

$$SR_i = \frac{\tilde{C}_{ij}}{\sum_j \tilde{C}_{ij}}.$$

A large self-recruitment (i.e., close to 1) means that the habitat is mostly isolated as it receives almost exclusively produced on the same habitat. It is therefore not resilient to disturbances. Finally, the average distance travelled by larvae originating from a given habitat can be computed with the weighted connectivity length:

$$WCL_i = \frac{\sum_j (d_{ij} \cdot \tilde{C}_{ij})}{\sum_j \tilde{C}_{ij}},$$

where is the distance between habitats *i* and *j*.

We also applied the strongly connected components (SCC) algorithm to the crab habitat connectivity graph to identify clusters of strongly connected habitats. The SCC method groups together habitats that are linked through bi-directional connections (Tarjan, 1972; Nuutila and Soisalon-Soininen, 1994). The communities created through this method do not depend on the strength of the connections but just on the existence of bi-directional connectivity pathways that connect any two habitats within the SCC, possibly through multistep connections. All the habitats within a SCC will thus have higher genetic mixing among them than with habitats in separate SCCs. The existence of closed-loop multi-generational connectivity pathways is a key factor that fosters population persistence (Hastings and Botsford, 2006).

2.3 Climate change scenarios

To evaluate the impacts of climate change, we run the larval dispersal model for three different scenarios. The first one corresponds to present-day conditions, with the water temperature simulated with the atmospheric conditions of 2019 and a pH of 8.075 (NOAA Ocean Acidification Program, 2020). The second scenario includes the effect of moderate climate change by assuming a uniform water temperature increase of 1°C as compared to present-day conditions and a uniform seawater pH of 7.8. This scenario corresponds to estimates for 2080-2100 under IPCC Representative Concentration Pathway (RCP) 2.6 scenario (Fox-Kemper et al., 2021). The third scenario represents the effect of an extreme climate change by assuming a water temperature increase of 3°C and a pH of 7.645, which would correspond to estimates for 2080-2100 under RCP 8.5 scenario.

Our model assumes that the effects of climate change, through water temperature increase and pH decrease, are only impacting crab larvae swimming activity and mortality. We did not consider the effect of climate change on the large-scale atmospheric and oceanic circulations, which could also influence larval dispersal in the region of interest. This simplification is due to the lack of precise information on projected changes in the wind regime over the Gulf of Mexico and the Loop Current dynamics. In a similar study on the effect of climate change on coral connectivity in the Great Barrier Reef, (Figueiredo et al., 2021) have shown that projected changes in ocean currents had a limited effect on larval dispersal.

3 Results

Our model shows that climate change will have two major effects on crab larvae by: 1) reducing the duration of the larval stages, and 2) limiting their vertical larval distribution in the water column (i.e., deeper distribution). The former effect is due to increasing temperature and the latter is due to decreasing pH. We illustrate these two effects by simulating the vertical position of an idealized crab larvae that would be driven only by its vertical swimming dynamics. Hydrodynamical effects are thus not considered. We assume that the larva is spawned at a depth of 60 m and the present-day temperature is 27°C (National Oceanic and Atmospheric Administration, 2021). In present-day conditions, the larva quickly reaches the surface and stays within about 10 meters from the surface until stage 4 when the individual moves towards the seabed (**Figure 3a**). The moderate climate change scenario is already strong enough to limit the larva's ability to swim near the surface. In this scenario, the larva stays within 20 to 40 meters from the bottom. The overall duration of the larval cycle is about 10% shorter (**Figure 3b**). In the case of extreme climate change, the larva never leaves the sea bottom

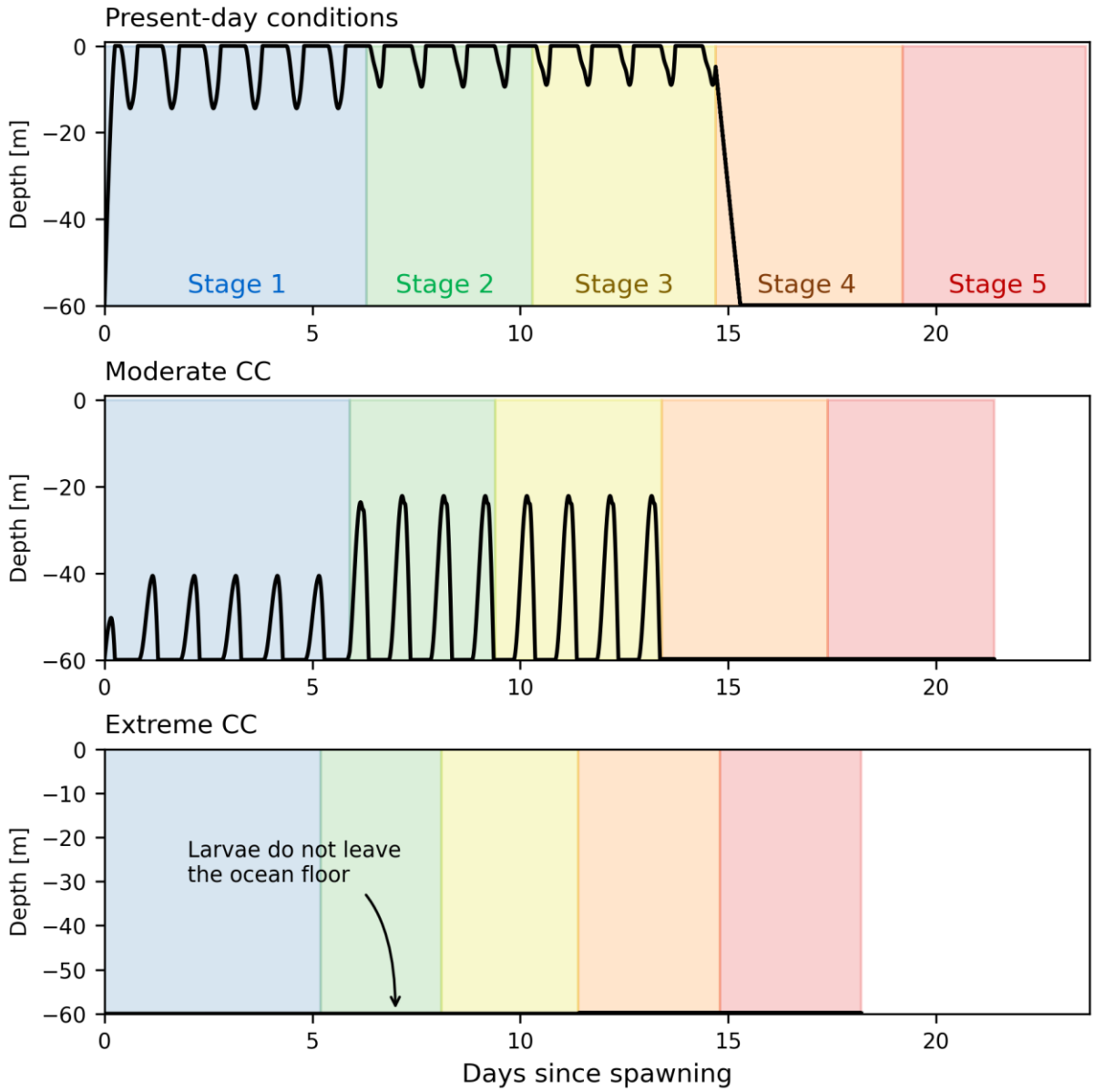

***Figure 3** : Theoretical vertical movements (black line) of a stone crab larva spawned at a depth of 60m through the five larval stages, according to different climate change scenarios. Each larval stage is represented by a different colour.*

throughout the entire larval stage. The duration of that cycle is further reduced by about 25% (**Figure 3c**).

When taking hydrodynamics into account, the combined effect of a temperature increase and a pH decrease reduces the dispersal distance of crab larvae on average by 15% (with standard deviation amongst habitats of 62%) for the moderate climate change scenario, and by 43% (SD = 44%) for extreme climate change scenario. These projected changes are however not spatially uniform as some habitats will experience much larger reductions in the distance at which larvae are dispersed. This seems to be particularly the case for habitats on the inner shelf (**Figure 4a**). An increase of WCL can be seen in some very localized parts of the domain.

The increase of the WCL observed around the FK in the extreme CC is paradoxically probably due the reduced dispersal distance of crab larvae. The FK are close to the limit of the domain, meaning that larvae can easily go out of the simulated area. In extreme climate change condition, larvae do not travel as far from their source habitat meaning that some larvae coming from around the FK might settle in the domain in the extreme scenario, when they went out of it in present day conditions.

When larval dispersal is limited, habitats become more isolated. Since larvae stay in their planktonic phase for about a month, many habitats experience a self-recruitment (SR) equal to 0, especially in the normal scenario (42% of the habitats have a SR of 0 in the normal scenario) where the larvae tend to travel farther away from their source habitat. This suggests that self-recruitment is not suitable to compute relative variations, as we would have to divide by 0 for almost half of the habitats. We decided instead to assess the absolute change of SR for both climate change scenarios. In the moderate climate change scenario, there is an increase of self-recruitment for 31% of the habitats, a decrease in 34% of the habitats, and no observable change in 32% of the habitats. During the extreme climate change simulations these percentages change to 58%, 19%, and 22% for the increase, decrease and no change in self-recruitment, respectively. These results suggest than in the extreme climate change scenario, the habitats become more isolated and fragmented. Again, these changes are not spatially uniform as there is a large inter-habitat variability meaning that some habitats will fare considerably worse than suggested by the average changes, and a small proportion of habitats will see an increase in recruitment (**Figure 4b**). The increase in self-recruitment is in general particularly important in the fishing area.

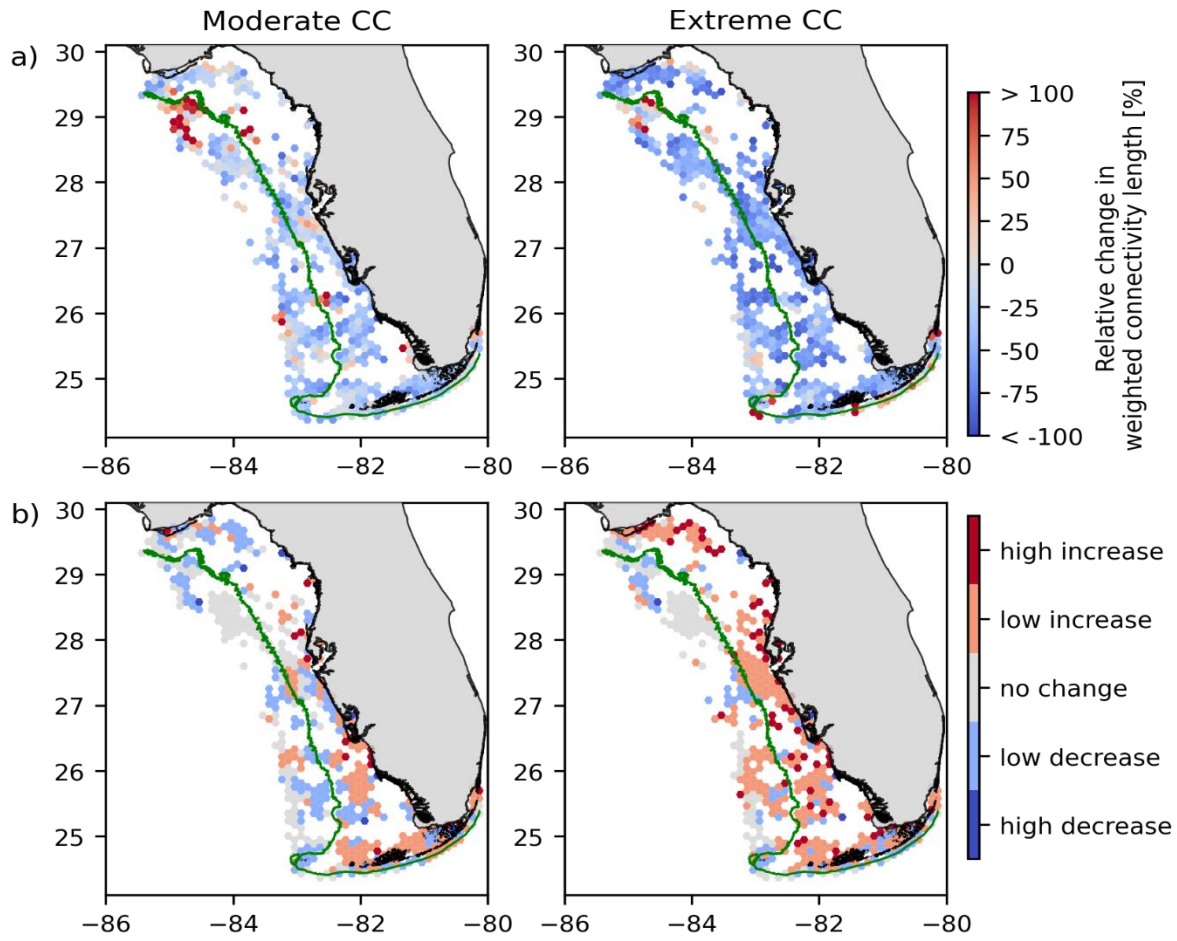

Figure 4 *: **(a)** Relative change in weighted connectivity length for both climate change scenarios and **(b)** absolute change in self-recruitment for both climate change scenarios. The green line represents the 30m-depth isobath separating the fishing and non-fishing zones.*

Interpreting the source index relative variations is complicated as this index is the product of the number of exported larvae with the number of outgoing connections. Those two indicators respond differently to climate change (**Figure 5a** and **Figure 5b**). The number of larvae that settle increases on average by 79% for the moderate climate change scenario and by 304% under the extreme climate change scenario. These increases are particularly marked for the habitats in the non-fishing zone (**Figure 5a**). Alternatively, the number of outgoing connections shows a mean relative decrease of 10% for moderate climate change scenarios and a 20% decrease for the extreme climate change scenario. Most of the habitats present this decreasing trend, even though there are some localized increases observed within the non-fishing zone. As a result of these two antagonistic reactions to climate change, the relative variation of the source index is difficult to interpret on its own. The general trend seems to be an increase of source index in the non-fishing zone (probably due to an increase in the number of larvae self-recruiting in the non-fishing zone) and a decrease of source index in the fishing zone (mainly due to a decrease in the number of out-going connections)(**Figure 5c**).

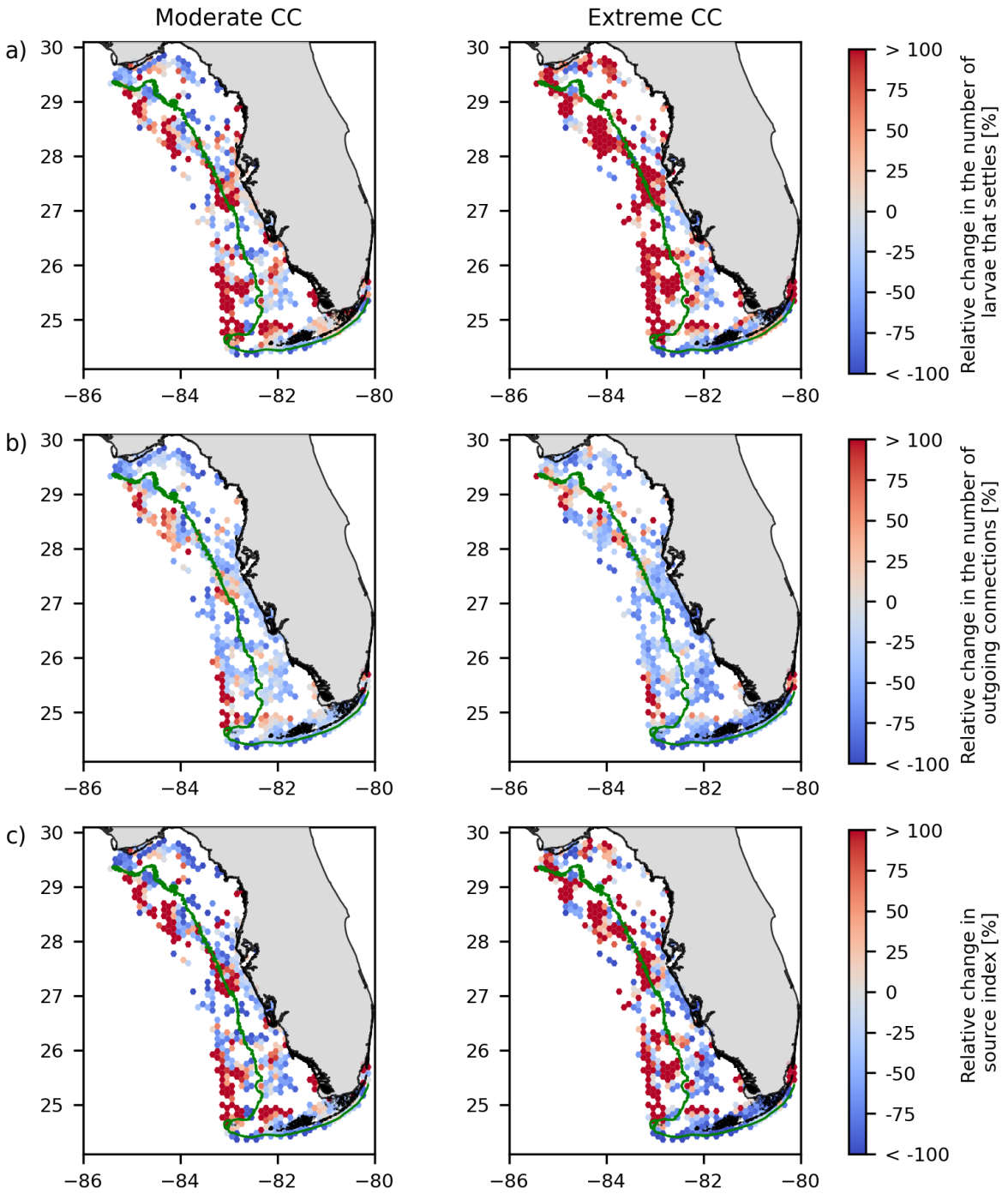

Figure 5 *: Relative change in* ***(a)*** *the number of larvae sent away that settle,* ***(b)*** *the number of outgoing connections with sink habitats and* ***(c)*** *the source index for both climate change scenarios compared to present-day values. The green line represents the separation between the fishing and non-fishing zones.*

The community structure obtained with the SCC algorithm confirms the overall increase in habitats isolation. The number of SCCs increases from 15 in present-day conditions to 18 and 53 for moderate and extreme climate change scenarios, respectively (**Figure 6**). As a result, the average number of habitats per community decreases by 54% for moderate climate change, and by 73 % in the extreme case. In the moderate CC scenario, this fragmentation leads to a separation of the FK community from the rest of the WFS communities. We also see the appearance of an area without communities to the northwest of the WFS. This means that none of the habitats in these zones are involved in a mutual

exchange of larvae with other habitats. In the extreme CC scenario, we observe a further breakdown of the communities, as well as a reappearance of communities in northwest area. The mechanism behind the appearance and disappearance of this northwest area without communities is difficult to pinpoint since it could be due to a combination of different factors including the variation of the currents speed and direction with depth, the fact that the larvae travel less of a distance with climate change stressor, or the orientation and positioning of the northwest habitats relatively to one another.

The proportion of larvae produced in a given habitat that eventually settle increases with the intensity

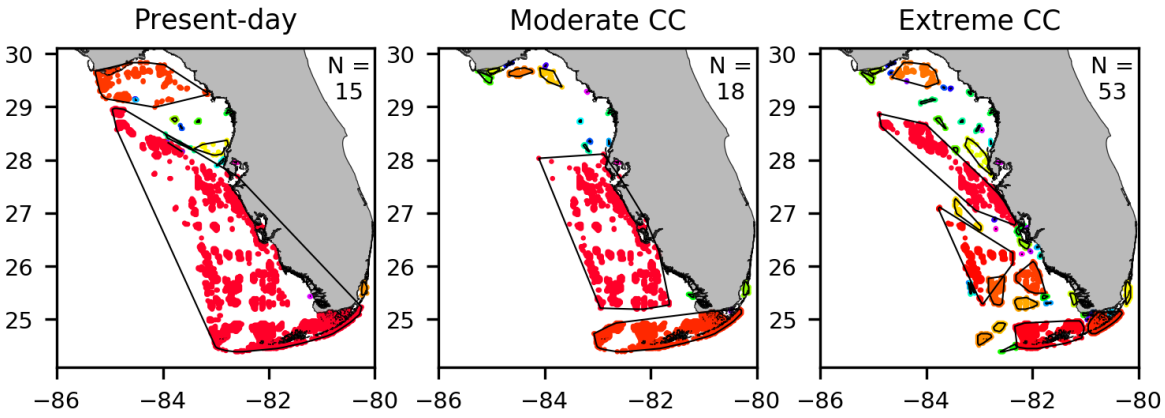

***Figure 6** : Map of the communities obtained with the SCC method for each climate change scenario. Each community is coloured in a different colour and is circled by a black line.*

of climate change (**Table 1**). This increase is mainly due to the increasing number of larvae that stay in the non-fishing zone (+ 183% between present-day conditions and extreme CC scenario). The increase in the number of larvae staying in the fishing zone due to climate change is less marked (+ 10%). We observe a decrease in the number of larvae staying in the fishing zone between the moderate and extreme scenarios. Even though the number of larvae traveling from the non-fishing zone to the fishing zone increases with climate change, they still represent only a small fraction of all the larvae exchanged.

***Table 1** : Percentage of larvae produced in the fishing (F) or non-fishing (NF) zones that settled in the fishing or non-fishing zones. The last column (Total) is the sum of the four others.*

	F to F	NF to F	F to NF	NF to NF	Total
Normal	0.52 %	0.02 %	0.01 %	0.12 %	0.67 %
Moderate CC	0.6 %	0.05 %	0.01 %	0.17 %	0.83 %
Extreme CC	0.57 %	0.05 %	0.01 %	0.34 %	0.97 %

4 Discussion and conclusions

Climate change will undoubtedly increase ocean temperatures and decrease the ocean pH. Our results show that those two effects will impact the dispersal and connectivity of stone crab larvae in three different ways. First, rising seawater temperatures will in a first time reduce larval mortality before increasing it when the ocean temperature will exceed larvae's optimum temperature. Second, increases in seawater temperatures will also reduce larval stage durations by up to 25 %. Finally, decreasing pH will impact larval stone crab's relative position in the water column by resulting in a deeper depth distribution. The combination of these three results will lead to an increase in the number of larvae that settle in some habitats but likely reduce the distance larvae can disperse. As a result, self-recruitment will increase, and habitat communities will become more fragmented along the WFS and throughout the FK. The spatial distribution of the Florida stone crab is also expected to change as southern and shallow habitats will be more impacted by increasing ocean temperature than northern and deeper habitats. This spatial shift in the stone crab distribution will impact the fishery, especially those in the southern part of the WFS such as in the FK.

Our model shows that stone crab larvae are expected to stay closer to the benthos and experience shorter larval stages during future climate scenarios. Both are known to reduce larval dispersion of several marine species (Shanks et al., 2003; North et al., 2008; Sundelöf and Jonsson, 2012). Since ocean currents weaken with greater depths, crab larvae will therefore be transported over shorter distances and will have a higher probability of settling within their natal habitat. Self-recruitment will thus increase and the size of habitat clusters that are connected through larval exchanges will decrease. The resulting smaller communities will be less resilient to external disturbances as all the habitat within a community could be impacted at the same time, potentially disrupting the populations ability to replenish the community. Species that have high dispersal capabilities and form large communities are indeed less vulnerable to sudden changes in external conditions and diseases due to higher genetic diversity and the potential of local recovery through larval transport (Hastings and Botsford, 2003; Jones et al., 2007).

Stone crab spatial distribution and abundance will also change. Temperature is a major factor influencing the fraction of larvae that successfully settles, as the mortality rate is function of the temperature. In our model of the present situation, the number of settlers is higher in southern and shallow areas, because water in northerner and deeper areas is too cold to allow high settlement during the first spawning events. With a small increase in the temperature, like in the moderate CC scenario, the proportion of larvae that settle increases throughout the entire WFS. However, for more extreme temperature increases, as could be observed by the end of the century, water temperature in shallow areas exceeds the larvae optimal temperature, leading to an increase in larval mortality compared to the moderate CC scenario. As a result, we expect that the stone crab larvae in the fishing zone will not significantly benefit from the increase in temperature. In addition, larvae produced in the non-fishing zone will likely benefit from the increase in water temperature, even for extreme CC. This suggests that climate change could lead to a shift in the stone crab abundance and distribution, with an increase of the number of larvae settling in deeper and northerner water, while the number of larvae settling in the shallower and southern area will stay rather constant. A shift to deeper or higher latitude water due to climate change has been observed for several marine species (Mieszkowska et al., 2006; Fujiwara et al., 2019) as well as other brachyuran crabs (Murphy, 2020). The number of larvae settling in the fishing zone will remain however larger than the number of larvae settling in the non-fishing zone.

Another consequence of the increase in water temperature is the increase in the number of larvae that settle. This increase will however not benefit the stone crab fishing industry. As mentioned above, the increase in the number of larvae settling will mainly happen in the non-fishing zone. In addition, the number of larvae going from the non-fishing zone to the fishing zone never exceeds 5% of the total amount of larvae exchanged, regardless of the scenario. This suggests that the non-fishing zone cannot serve as a source of larvae for the habitats within the fishing zone.

As for every model study, this work was based on different assumptions. Due to lack of more accurate data, we could not completely represent all the processes driving the vertical larval dynamics for the 5 different larval stages of the stone crab. This could be improved by conducting vertically stratified plankton surveys to estimate vertical velocities according to larval depth distribution, like in Peliz et al. (2007). Furthermore, there is also some uncertainty on the location of crab habitats. For lack of better data, we assumed that all rocky, muddy or gravely substrates shallower than 60 m would be suitable for stone crabs. This is probably an overestimation of the actual crab habitats. Habitat maps could be refined by following the approach of Criales et al. (2019) who backtracked larvae from locations where crabs have been observed to identify their source habitat. Another limitation is that we did not take the spatial heterogeneity of pH, pH decreases, and temperature increases into account. We assumed a constant value of water pH over the entire WFS, while it is known that it varies both horizontally (NOAA Ocean Acidification Program, 2020) and vertically (Byrne et al., 2010). Likewise, in the climate change scenarios, we decreased (resp. increased) the water pH (resp. temperature) by a constant over the entire domain, while these changes are probably not going to be spatially homogeneous. We also assumed that the oceanic and atmospheric circulation would remain the same for the different CC scenarios. This assumption is supported by the study of Figueiredo et al. (2021) on coral connectivity changes in the Great Barrier Reef due to climate change. They found that changes in the hydrodynamics have a much weaker effect than changes in larval biology on connectivity. Finally, while we considered several spawning events, we did not consider multiple years to explicitly take interannual variability into account. This is mostly due to the heavy computational cost for running high-resolution three-dimensional simulations over the entire WFS.

Despite these limitations, our model brings unprecedented perspectives on the impact climate change will have on the stone crab population along the WFS and within the FK. As the first model to evaluate the current and future dispersion of *M. mercenaria*, this work could help local authorities to understand the mechanisms underlying stone crab distribution and population connectivity which is beneficial if fisheries management is to prepare for future changes in climate. Our work could also serve as a reference for other studies aiming to model the dispersion of brachyuran crabs. Brachyuran crabs are found all around the world, in almost all coastal habitats, with many species being commercially important (Azra et al., 2020). In this work we introduced several new elements compared to other dispersal models of brachyuran crabs, like the sinusoidal response to light (more realistic than a binary up and down vertical swimming behavior) or the pH-dependent vertical velocity component that allowed to evaluate the impacts of ocean acidification on the stone crabs distribution. Since all brachyuran crabs respond to external stimuli like hydrostatic pressure and light (Epifanio and Cohen, 2016), our approach could be used to estimate their dispersion patterns.

5 Data Availability Statement

The datasets generated for this study are available on request to the corresponding author.

6 Conflict of Interest

The authors declare that the research was conducted in the absence of any commercial or financial relationships that could be construed as a potential conflict of interest.

7 Author Contributions

LA developed the model, ran the simulations, and analyzed the results. EH conceptualized the study and designed the modeling experiments. PG collected and analyzed the biological data. TD developed the model. All authors contributed to the writing of the manuscript.

8 Funding

Gravinese's research is supported by an U.S. National Science Foundation Biological Oceanography Grant (award number OCE-2049047).

9 Acknowledgments

Computational resources were provided by the Consortium des Équipements de Calcul Intensif (CÉCI), funded by the F.R.S.-FNRS under Grant No. 2.5020.11. LA is a Ph.D. student supported by the Fund for Research Training in Industry and Agriculture (FRIA/FNRS).

10 References

Azra, M. N., Aaqillah-Amr, M. A., Ikhwanuddin, M., Ma, H., Waiho, K., Ostrensky, A., et al. (2020). Effects of climate-induced water temperature changes on the life history of brachyuran crabs. *Rev. Aquac.* 12, 1211–1216. doi:https://doi.org/10.1111/raq.12380.

Baeza, J., Holstein, D., Umaña-Castro, R., and Mejía-Ortíz, L. (2019). Population genetics and biophysical modeling inform metapopulation connectivity of the Caribbean king crab Maguimithrax spinosissimus. *Mar. Ecol. Prog. Ser.* 610, 83–97. doi:10.3354/meps12842.

Banas, N. S., McDonald, P. S., and Armstrong, D. A. (2009). Green Crab Larval Retention in Willapa Bay, Washington: An Intensive Lagrangian Modeling Approach. *Estuaries Coasts* 32, 893–905.

Beck, M. W. (1995). Size-Specific Shelter Limitation in Stone Crabs: A Test of The Demographic Bottleneck Hypothesis. *Ecology* 76, 968–980.

Bednaršek, N., Ambrose, R., Calosi, P., Childers, R. K., Feely, R. A., Litvin, S. Y., et al. (2021). Synthesis of Thresholds of Ocean Acidification Impacts on Decapods. *Front. Mar. Sci.* 8, 1542. doi:10.3389/fmars.2021.651102.

Bert, T. M., Warner, R. E., and Kessler, L. D. (1978). The biology and florida fishery of the stone crab, Menippe mercenaria (Say), with emphasis on southwest florida. Available at: https://ufdc.ufl.edu/UF00072275/00001/1j.

Brown, S. D., Bert, T. M., Tweedale, W. A., Torres, J. J., and Lindberg, W. J. (1992). The effects of temperature and salinity on survival and development of early life stage Florida stone crabs Menippe mercenaria (Say). *J. Exp. Mar. Biol. Ecol.* 157, 115–136.

Byrne, R. H., Mecking, S., Feely, R. A., and Liu, X. (2010). Direct observations of basin-wide acidification of the North Pacific Ocean. *Geophys. Res. Lett.* 37. Available at: https://agupubs.onlinelibrary.wiley.com/doi/abs/10.1029/2009GL040999 [Accessed June 2, 2021].

Ceballos-Osuna, L., Carter, H. A., Miller, N. A., and Stillman, J. H. (2013). Effects of ocean acidification on early life-history stages of the intertidal porcelain crab Petrolisthes cinctipes. *J. Exp. Biol.* 216, 1405–1411.

Cowen, R. K., and Sponaugle, S. (2009). Larval Dispersal and Marine Population Connectivity. *Annu. Rev. Mar. Sci.* 1, 443–466.

Criales, M. M., Cherubin, L., Gandy, R., Garavelli, L., Ghannami, M., and Crowley, C. (2019). Blue crab larval dispersal highlights population connectivity and implications for fishery management. *Mar. Ecol. Prog. Ser.* 625.

Dissanayake, A., and Ishimatsu, A. (2011). Synergistic effects of elevated CO2 and temperature on the metabolic scope and activity in a shallow-water coastal decapod (Metapenaeus joyneri; Crustacea: Penaeidae). *ICES J. Mar. Sci.* 68, 1147–1154. doi:10.1093/icesjms/fsq188.

Dubois, M., Rossi, V., Ser-Giacomi, E., Arnaud-Haond, S., López, C., and Hernández-García, E. (2016). Linking basin-scale connectivity, oceanography and population dynamics for the conservation and management of marine ecosystems. *Glob. Ecol. Biogeogr.* 25, 503–515. doi:10.1111/geb.12431.

Duquesne, F., Vallaeys, V., Vidaurre, P. J., and Hanert, E. (2021). A coupled ecohydrodynamic model to predict algal blooms in Lake Titicaca. *Ecol. Model.* 440, 109418. doi:10.1016/j.ecolmodel.2020.109418.

Egbert, G., and Erofeeva, S. (2002). Efficient Inverse Modeling of Barotropic Ocean Tides. *J. Atmospheric Ocean. Technol.* 19, 183–204.

Epifanio, C. E., and Cohen, J. H. (2016). Behavioral adaptations in larvae of brachyuran crabs: A review. *J. Exp. Mar. Biol. Ecol.* 482, 85–105.

Figueiredo, J., Thomas, C. J., Deleersnijder, E., Lambrechts, J., Baird, A. H., Connoly, S. R., et al. (2021). Global warming weakens connectivity among coral populations. *Nat. Clim. Change Rev.*

Florida Fish and Wildlife Conservation Commission (1998). Public Fisheries-Dependent Monitoring: Commercial Fisheries Landings Summaries. Available at: https://public.myfwc.com/FWRI/PFDM/ReportCreator.aspx [Accessed August 5, 2021].

Fox-Kemper, B., Hewitt, H. T., Xiao, C., Aðalgeirsdóttir, G., Drijfhout, S. S., Edwards, T. L., et al. (2021). "Ocean, Cryosphere and Sea Level Change," in *Climate Change 2021: The Physical Science Basis. Contribution of Working Group I to the Sixth Assessment Report of the Intergovernmental Panel on Climate Chang* IPCC. Available at: https://www.ipcc.ch/report/ar6/wg1/#FullReport.

Fujiwara, M., Martinez-Andrade, F., Wells, R. J. D., Fisher, M., Pawluk, M., and Livernois, M. C. (2019). Climate-related factors cause changes in the diversity of fish and invertebrates in subtropical coast of the Gulf of Mexico. *Commun. Biol.* 2, 1–9.

GBIF Backbone Taxonomy (2019). Menippe mercenaria (Say, 1818). *GBIF Secr.* Available at: https://www.gbif.org/species/5178757 [Accessed March 13, 2021].

Gravinese, P. M. (2018). Vertical swimming behavior in larvae of the Florida stone crab, Menippe mercenaria. *J. Plankton Res.* 40, 643–654.

Gravinese, P. M., Enochs, I. C., Manzello, D. P., and van Woesik, R. (2018). Warming and pCO2 effects on Florida stone crab larvae. *Estuar. Coast. Shelf Sci.* 204, 193–201.

Gravinese, P. M., Enochs, I. C., Manzello, D. P., and van Woesik, R. (2019). Ocean acidification changes the vertical movement of stone crab larvae. *Biol. Lett.* 15, 1–7.

Gulf Shores Marine Fisheries Commission (2001). Summary table of the Stone Crab, *Menippe mercenaria*,: Life History for the Gulf of Mexico. Gulf Shores Marine Fisheries Commission Available at: http://www.gsmfc.org/pubs/habitat/tables/stonecrab.pdf [Accessed October 1, 2020].

Hastings, A., and Botsford, L. (2003). Comparing designs of marine reserves for fisheries and for biodiversity. *Ecol. Appl. - ECOL APPL* 13, 65–70.

He, R., and Weisberg, R. H. (2002). West Florida shelf circulation and temperature budgetfor the 1999 spring transition. *Cont. Shelf Res.* 22, 719–748.

He, R., and Weisberg, R. H. (2003). West Florida shelf circulation and temperature budget for the 1998 fall transition. *Cont. Shelf Res.* 23, 777–800.

Hoegh-Guldberg, O., Cai, R., Poloczanska, E. S., Brewer, P. G., Sundby, S., Hilmi, K., et al. (2014). "The Ocean," in (Cambridge, United Kingdom and New York, NY, USA: Cambridge University Press), 1655–1731.

INSTAAR, U. of C. (2011). Seafloor Substrates Griddings, Gulf of Mexico.

Jones, G., Srinivasan, M., and Almany, G. (2007). Population Connectivity and Conservation of Marine Biodiversity. *Oceanogr. Wash. DC* 20, 100–111.

Kool, J. T., Moilanen, A., and Treml, E. A. (2013). Population connectivity: recent advances and new perspectives. *Landsc. Ecol.* 28, 165–185. doi:10.1007/s10980-012-9819-z.

Krimsky, L. S., and Epifanio, C. E. (2008). Multiple cues from multiple habitats : Effect of metamorphosis of the Florida ston crab, Menippe mercenaria. *J. Exp. Mar. Biol. Ecol.* 358, 178–184.

Kuhn, A. A. (2017). Effects of Temperature on Growth and Molting in Blue Crabs Effects of Temperature on Growth and Molting in Blue Crabs (Callinectes Sapidus) and Lesser Blue Crabs ((Callinectes Sapidus) and Lesser Blue Crabs (Callinectes similisCallinectes similis)). Available at: https://aquila.usm.edu/cgi/viewcontent.cgi?article=1361&context=masters_theses.

Kurihara, H. (2008). Effects of CO2-driven ocean acidification on the early developmental stages of invertebrates. *Mar. Ecol. Prog. Ser.* 373, 275–284.

Lindberg, W. J., and Marshall, M. J. (1984). Species Profiles: Life Histories and Environmental Requirements of Coastal Fishes and Invertebrates (South Atlantic): Stone Crab. Washington

(D.C.): Florida Gulf Coast University Available at: https://fgcu.digital.flvc.org/islandora/object/fgcu%3A27184.

Liu, Y., and Weisberg, R. H. (2012). Seasonal variability on the West Florida Shelf. *Prog. Oceanogr.* 104, 80–98.

Metzger, R., Sartoris, F. J., Langenbuch, M., and Pörtner, H. O. (2007). Influence of elevated CO2 concentrations on thermal tolerance of the edible crab Cancer pagurus. *J. Therm. Biol.* 32, 144–151. doi:10.1016/j.jtherbio.2007.01.010.

Mieszkowska, N., Kendall, M. A., Hawkins, S. J., Leaper, R., Williamson, P., Hardman-Mountford, N. J., et al. (2006). "Changes in the range of some common rocky shore species In Britain — A Response To Climate Change?," in *Marine Biodiversity: Patterns and Processes, Assessment, Threats, Management and Conservation* Developments in Hydrobiology., eds. K. Martens, H. Queiroga, M. R. Cunha, A. Cunha, M. H. Moreira, V. Quintino, et al. (Dordrecht: Springer Netherlands), 241–251. doi:10.1007/1-4020-4697-9_20.

Minor, E. S., and Urban, D. L. (2007). Graph Theory as a Proxy for Spatially Explicit Population Models in Conservation Planning. *Ecol. Appl.* 17, 1771–1782. doi:10.1890/06-1073.1.

Muller, R. G., Chagaris, D., Bert, T. M., Crawford, C., and Gandy, R. (2011). The 2011 Stock Assessment Update for the Stone Crab, Menippe spp., Fishery in Florida. St. Petersburg, Florida.: Fish and Wildlife Research Institute, Florida Fish And Wildlife Conservation Commission Available at: http://myfwc.com/research/saltwater/crustaceans/stone-crabs/stock-assessments/ [Accessed April 21, 2021].

Murphy, J. T. (2020). Climate change, interspecific competition, and poleward vs. depth distribution shifts: Spatial analyses of the eastern Bering Sea snow and Tanner crab (Chionoecetes opilio and C. bairdi). *Fish. Res.* 223, 105417. doi:10.1016/j.fishres.2019.105417.

National Oceanic and Atmospheric Administration (2021). National Data Buoy Center. Available at: https://www.ndbc.noaa.gov/ [Accessed October 15, 2020].

NOAA National Geophysical Data Center (2001). U.S. Coastal Relief Model Vol.3 - Florida and East Gulf of Mexico.

NOAA Ocean Acidification Program (2020). Ocean Acidification Product Suite : The Caribbean Sea and Gulf of Mexico. *NOAA - Coral Health Monit. Program*. Available at: https://www.coral.noaa.gov/accrete/oaps.html [Accessed May 20, 2021].

North, E., Schlag, Z., Hood, R., Li, M., Zhong, L., Gross, T., et al. (2008). Vertical swimming behavior influences the dispersal of simulated oyster larvae in a coupled particle-tracking and hydrodynamic model of Chesapeake Bay. *Mar. Ecol.-Prog. Ser. - MAR ECOL-PROGR SER* 359, 99–115. doi:10.3354/meps07317.

Nuutila, E., and Soisalon-Soininen, E. (1994). On finding the strongly connected components in a directed graph. *Inf. Process. Lett.* 49, 9–14.

Okubo, A. (1971). Oceanic diffusion diagrams. *Deep Sea Res. Oceanogr. Abstr.* 18, 789–802.

Peliz, A., Marchesiello, P., Dubert, J., Marta-Almeida, M., Roy, C., and Queiroga, H. (2007). A study of crab larvae dispersal on the Western Iberian Shelf: Physical processes. *J. Mar. Syst.* 68, 215–236.

Pineda, J., Hare, J. A., and Sponaugle, S. (2007). Larval transport and dispersal in the coastal ocean and consequences for population connectivity. *Oceanography* 20, 22–39.

Pires, R. F. T., Peliz, Á., Pan, M., and dos Santos, A. (2020). "There and back again" − How decapod megalopae find the way home: A modelling exercise for Pachygrapsus marmoratus. *Prog. Oceanogr.* 184, 102331. doi:10.1016/j.pocean.2020.102331.

Porter, H. J. (1960). Zoeal Stages of the Stone Crab, Menippe mercenaria Say. *Chesap. Sci.* 1, 168.

Rayfield, B., Fortin, M.-J., and Fall, A. (2011). Connectivity for conservation: a framework to classify network measures. *Ecology* 92, 847–858. doi:10.1890/09-2190.1.

Seyoum, S., Gandy, R. L., Crowley, C. E., and Puchulutegui, C. (2021). A novel interpretation of speciation, hybridization, and genetic population structure of the stone crabs Menippe mercenaria (Say, 1817–1818) and M. adina Williams & Felder, 1986 (Decapoda: Brachyura: Menippidae). *J. Crustac. Biol.* 41. doi:10.1093/jcbiol/ruab018.

Shanks, A. L., Grantham, B. A., and Carr, M. H. (2003). Propagule Dispersal Distance and the Size and Spacing of Marine Reserves. *Ecol. Appl.* 13, 159–169. doi:https://doi.org/10.1890/1051-0761(2003)013[0159:PDDATS]2.0.CO;2.

Smagorinsky, J. (1963). General circulation experiments with the primitive equations : I. The basic experiment. *Mon. Weather Rev.* 91, 99–164.

Smith, S. D., and Banke, E. G. (1975). Variation of the sea surface drag coefficient with wind speed. *Q. J. R. Meteorol. Soc.* 101, 665–673.

Sulkin, S. D. (1984). Behavioral basis of depth regulation in the larvae of brachyuran cra. *Mar. Ecol. Prog. Ser.* 15, 181–205.

Sundelöf, A., and Jonsson, P. R. (2012). Larval dispersal and vertical migration behaviour – a simulation study for short dispersal times. *Mar. Ecol.* 33, 183–193. doi:https://doi.org/10.1111/j.1439-0485.2011.00485.x.

Tarjan, R. (1972). Depth-First Search and Linear Graph Algorithms. *SIAM J. Comput.* 1, 146–160.

Vallaeys, V., Kärnä, T., Delandmeter, P., Lambrechts, J., Baptista, A. M., Deleersnijder, E., et al. (2018). Discontinuous Galerkin modeling of the Columbia River's coupled estuary-plume dynamics. *Ocean Model.* 124, 111–124.

Vallaeys, V., Lambrechts, J., Delandmeter, P., Pätsch, J., Spitzy, A., Hanert, E., et al. (2021). Understanding the circulation in the deep, micro-tidal and strongly stratified Congo River estuary. *Ocean Model.* 167, 101890. doi:10.1016/j.ocemod.2021.101890.

Weisberg, R. H., Li, Z., and Muller-Karger, F. (2001). West Florida shelf response to local wind forcing: April 1998. *J. Geophys. Res. Oceans* 106, 31239–31262.

Young, A. M., and Hazlett, T. L. (1978). The effect of salinity and temperature on the larval development of clibanarius vittatus (Bosc) (crustacea: decapoda: diogenidae). *J. Exp. Mar. Biol. Ecol.* 34, 131–141.

11 Appendix

11.0 Hydrodynamic model formulation

SLIM3D is an ocean model that solves the 3D hydrostatic equations under the Boussinesq approximation (Vallaeys et al., 2018, 2021; Duquesne et al., 2021). The model equations read:

$$\frac{\partial \boldsymbol{u}}{\partial t} + \boldsymbol{\nabla}_h \cdot (\boldsymbol{u}\boldsymbol{u}) + \frac{\partial w\boldsymbol{u}}{\partial z} = \boldsymbol{\nabla}_h \cdot \left(v_h(\boldsymbol{\nabla}_h \boldsymbol{u} + (\boldsymbol{\nabla}_h \boldsymbol{u})^T)\right) + \frac{\partial}{\partial z}\left(v\frac{\partial \boldsymbol{u}}{\partial z}\right) - f\boldsymbol{e}_z \times \boldsymbol{u} - \frac{1}{\rho_0}\boldsymbol{\nabla}_h p, \quad (1)$$

$$\boldsymbol{\nabla}_h \cdot \boldsymbol{u} + \frac{\partial w}{\partial z} = 0, \quad (2)$$

$$\frac{1}{\rho_0}\boldsymbol{\nabla}_h p = \frac{1}{\rho_0}\boldsymbol{\nabla}_h p_a + g\boldsymbol{\nabla}_h \eta + \frac{g}{\rho_0}\boldsymbol{\nabla}_h \int_z^\eta (\rho - \rho_0)\, dz, \quad (3)$$

$$\frac{\partial T}{\partial t} + \boldsymbol{\nabla}_h \cdot (\boldsymbol{u}T) + \frac{\partial (wT)}{\partial z} = \boldsymbol{\nabla}_h \cdot (\kappa_h \boldsymbol{\nabla}_h T) + \frac{\partial}{\partial z}\left(\kappa\frac{\partial T}{\partial z}\right) + f_{relaxT}, \quad (4)$$

$$\frac{\partial S}{\partial t} + \boldsymbol{\nabla}_h \cdot (\boldsymbol{u}S) + \frac{\partial (wS)}{\partial z} = \boldsymbol{\nabla}_h \cdot (\kappa_h \boldsymbol{\nabla}_h S) + \frac{\partial}{\partial z}\left(\kappa\frac{\partial S}{\partial z}\right) + f_{relaxS}, \quad (5)$$

where **u** is the horizontal velocity, composed of the zonal and meridional velocity components, w is the vertical velocity, $\boldsymbol{\nabla}_h$ is the horizontal gradient operator, v_h is the horizontal viscosity parametrized with Smagorinsky's turbulence model (Smagorinsky, 1963), T is the temperature, v is the vertical eddy viscosity computed with GOTM (General Ocean Turbulence Model), f is the Coriolis factor, $\boldsymbol{e}_z$ is the vertical unit vector, ρ_0 is the reference density, p is the pressure, p_a is the atmospheric pressure, η is the elevation, ρ is the density, κ_h is the horizontal eddy diffusivity defined by the Okubo parametrization (Okubo, 1971), κ is the vertical eddy diffusivity computed with GOTM and f_{relaxT} and f_{relaxS} are respectively the temperature and salinity relaxation terms expressed as:

$$f_{relax\,Y} = -\frac{max(z_r + z, 0)}{z_r t_{relax}} * (Y - Y_{ext})$$

where z_r = 12 m is the surface layer thickness, t_{relax} = 5 days is the relaxation time, Y is either T or S and Y_{ext} is the value of variable Y at the ocean surface as computed by the HYbrid Coordinate Ocean Model (HYCOM).

The current velocity and sea surface elevation imposed on the open boundaries are a combination of tides provided by the OSU TOPEX/Poseidon Global Inverse Solution dataset TPXO9 (Egbert and Erofeeva, 2002) and the large-scale circulation computed with HYCOM-GOM.

The bottom and surface boundaries are made impermeable through the following equations:

$$w + \boldsymbol{u} \cdot \boldsymbol{\nabla}_h h = 0 \quad (6)$$

$$w - \frac{\partial \eta}{\partial t} - \boldsymbol{u} \cdot \boldsymbol{\nabla}_h \eta = 0 \quad (7)$$

There is an input of momentum at the surface from the wind and a dissipation of momentum at the bottom from friction. These two fluxes are expressed as follows:

$$v\frac{\partial \boldsymbol{u}}{\partial z} = \frac{\tau_s}{\rho_0} \quad (8)$$

$$\nu \frac{\partial \boldsymbol{u}}{\partial z} = \frac{\tau_b}{\rho_0} \tag{9}$$

where τ_s is the surface wind stress and τ_b is the bottom friction stress. The wind stress is derived from Smith and Banke (1975), based on the 10-m wind velocity provided by ERA5. The bottom friction is computed with the law of the wall, assuming a logarithmic velocity profile characterized by a roughness height z_0.

Initially, the velocity and the sea surface elevation are set to zero, and the temperature and salinity are set to HYCOM's value. This means that the model needs a few days to spin-up and reach a dynamical equilibrium. For this reason, we chose to start the hydrodynamic simulation on April 15th, while the larval dispersal simulation only starts on May 1st.

11.1 Hydrodynamic model validation

To validate the outputs of the model, they were compared with observations collected at three NOAA stations (**Figure 1a**). The simulated current velocity output was compared to observations at a 4 m depth at the station 42023 (26.010° N, 83.086° W). Concerning the temperature and salinity, the outputs were respectively compared with the observations at a 1 m depth at station 42013 (27.173°N, 82.924°W), and station 42022 (27.505°N, 83.741°W). The stations were chosen because they had the best record of observations (i.e. few missing values) during the simulated period.

The horizontal current velocity simulated with SLIM 3D from May to September 2019 compares well to observations at station 42023 **(Figure 7a-d)**. We also compared SLIM model outputs with HYCOM's output **(Figure 7e)** and put them both in perspective with the wind forcing from ERA5 **(Figure 7f)**. All these sources have been resampled to compare them at the same time points. Overall, SLIM correctly reproduces the currents direction and amplitude. It tends however to produce currents that are more northward than the observations. There are also two more intense southward current events observed in June and July that SLIM does not reproduce. The origin of these two events remains unclear as they do not show up in the wind field. SLIM's slight northward bias is probably due to the HYCOM forcing on the boundaries. As can be seen in **Figure 7** , HYCOM produces a strong northward dynamics that does not agree well with observations.

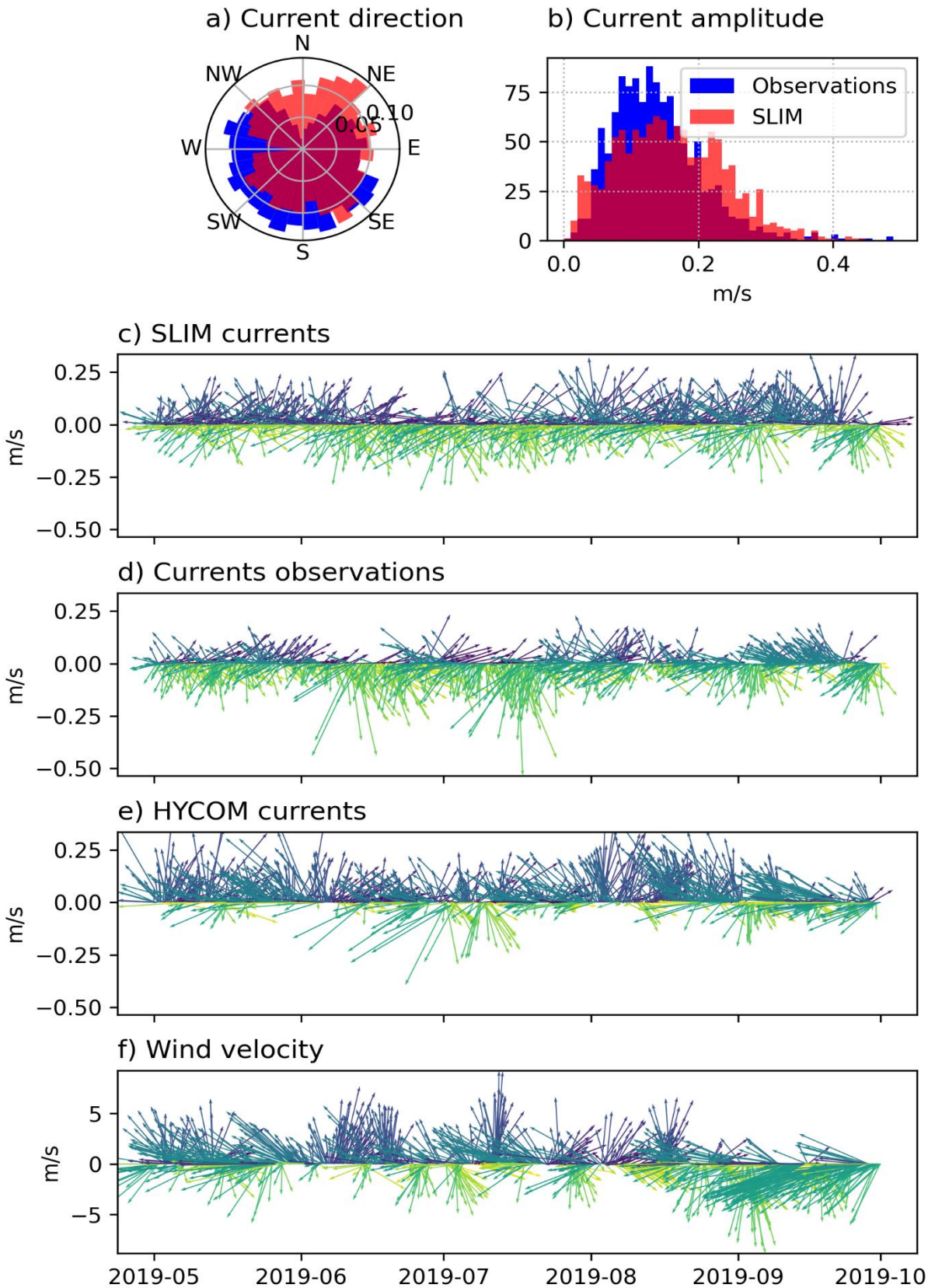

Figure 7 : Comparison of the horizontal velocity outputs of SLIM with observations from the NOAA and forcings from HYCOM and ERA5 (wind velocity) from May to September 2019. The currents are measured and modeled four meters below the surface at station 42023 (26.010° N and 83.086° W). The wind velocities are modeled 10 meters above the surface at the same coordinates. The first two graphs are histograms of the direction and amplitudes of the currents comparing SLIM with observations. The four other plots present the evolution of the horizontal velocities throughout the study period (an arrow pointing up represent a northward current). The color stresses the direction of the currents

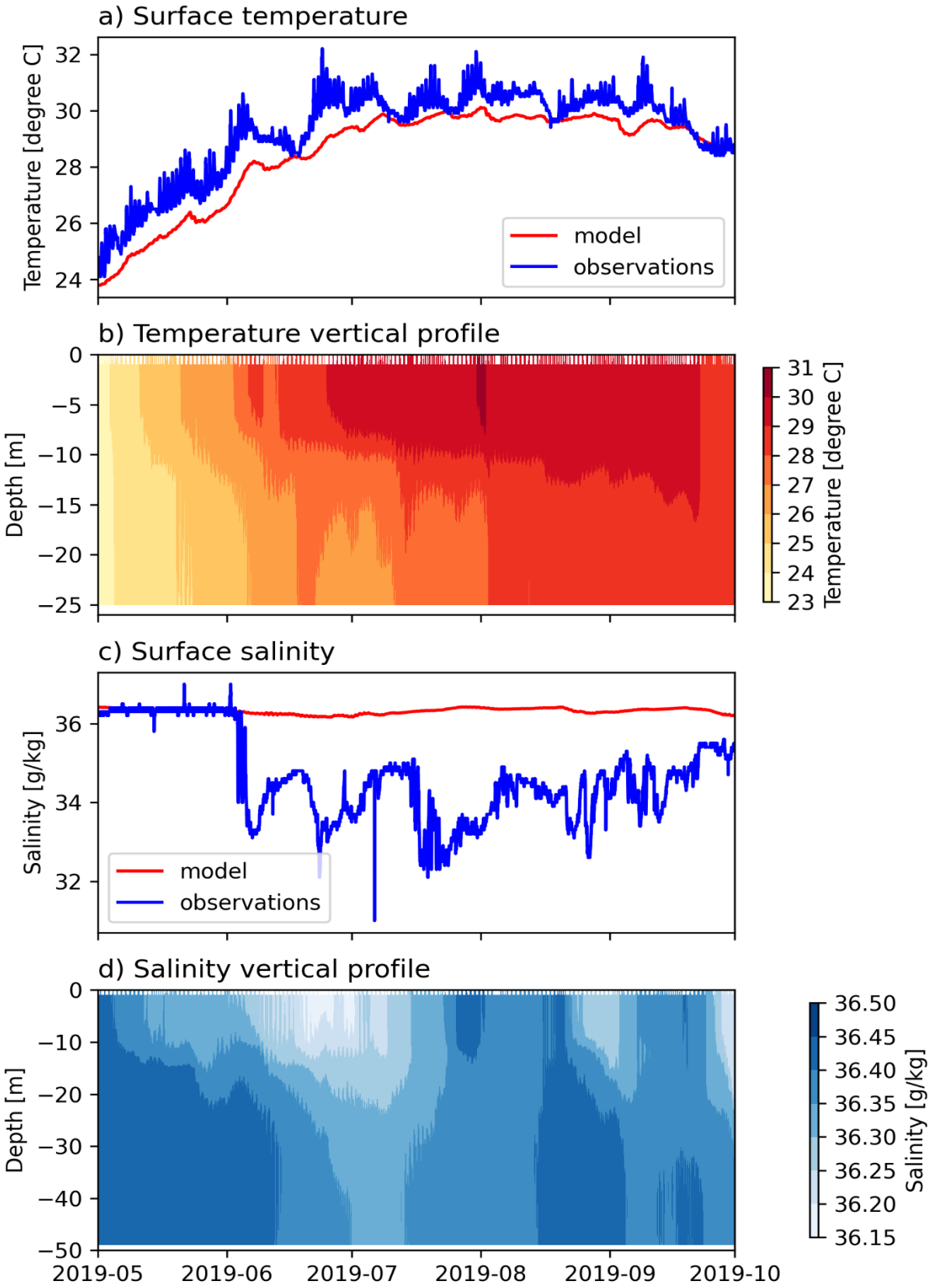

Figure 8 : Validation of temperature and salinity outputs of SLIM. First and third graphs show respectively SLIM's temperature and salinity one meter below the surface, compared with observations at the same point. The second and last graphs show the evolution of the temperature and salinity with time and depth. The point of validation for the temperature and salinity are respectively 27.173°N - 82.924°W and 27.505°N- 83.741°W

Regarding the temperature, the comparison between SLIM's output and NOAA's observations can be found in **Figure 8**. Even though SLIM tends to slightly underestimate the water temperature **(Figure 8a)**, it follows the right seasonal trend. We can also observe a transition from a horizontal to a vertical temperature stratification by the beginning of summer **(Figure 8b)**, which is typical of mid-latitude continental shelves and has been observed on the WFS (He and Weisberg, 2002, 2003). Overall, SLIM's salinity outputs of SLIM appear to be relatively constant, both over time and depth **(Figure 8c-d)**. SLIM does not represent the decrease in salinity observed in June. This lack of variability is due to the HYCOM forcing that we use to force the salinity on the model surface and lateral boundaries.

11.2 Larval transport model

To model larval dispersal, we used SLIM's Lagrangian particle tracker (LPT). The movement of the particles is obtained by combining the larval swimming velocity with the currents velocity to obtain $\boldsymbol{u_L}$, the total larval velocity. This velocity vector is then injected in a 3D advection-diffusion equation expressed in Lagrangian form:

$$d\boldsymbol{X}(t) = (\boldsymbol{u_L} + \boldsymbol{\nabla} \cdot \boldsymbol{K})dt + \sqrt{2\boldsymbol{K}}d\boldsymbol{W}(t) \quad (10)$$

where $d\boldsymbol{W}(t)$ is a Wiener noise increment, and

$$\boldsymbol{K} = \begin{bmatrix} \kappa_{L,h} & 0 & 0 \\ 0 & \kappa_{L,h} & 0 \\ 0 & 0 & \kappa_L \end{bmatrix}$$

is the diffusivity tensor where $\kappa_{L,h}$ is the horizontal diffusivity defined by the Okubo parametrization (Okubo, 1971) and κ_L is the vertical diffusivity that takes the same value as the temperature and salinity vertical diffusivities. Eq. (10) is then solved numerically by the means of a 4th order Runge Kutta scheme.

The biological component of the larval vertical velocity is expressed as:

$$w_B = \alpha_p \cdot (w_d + w_{Li} + w_{pH})$$

where α_p is a corrective factor due to a response to pressure, w_d is the downward swimming velocity and w_{Li} and w_{pH} are the vertical velocity in response to light and pH respectively. Since the different stages react differently to external stimuli, we defined the vertical velocity of each stage separately (Table 2).

Table 2 : Components of the vertical velocity of the different life stages.

Life stage	Vertical velocity [m/s]
Larval stage -1	$w_{B,1} = \alpha_{p,1} \cdot (w_{Li,1} + w_{pH,1})$
Larval stage -2	$w_{B,2} = \alpha_{p,2} \cdot (w_{Li,2} + w_{pH,2})$
Larval stage -3	$w_{B,3} = \alpha_{p,3} \cdot (w_{Li,3} + w_{pH,3})$
Larval stage -4	$w_{B,4} = \alpha_{p,4} \cdot w_{d,4}$
Larval stage -5	$w_{B,5} = \alpha_{p,5} \cdot w_{d,5}$
Megalopal stage	$w_{B,M} = w_{d,M}$

Larvae's response to light was defined by using the time of the day for larval stages -1 to -3:

$$w_{Li} = \left(w_{d,i} - \left(w_{u,i} - w_{d,i}\right) \cdot \left(\left(\Delta t_m // (12 \cdot 3600)\right)\%2\right)\right) \cdot sin\left(\frac{2\pi}{24 \cdot 3600} \cdot (\Delta t_m)\right) \quad (11)$$

where $w_{d,i}$ is the mean downward velocity of stage i larvae according to Gravinese (2018), $w_{u,i}$ is the upward swimming velocity of stage i, $\Delta t_m = t_m - 6 \cdot 3600$ where t_m is the time since midnight in seconds, // is the floor division operator and % is the modulo operator. Larval stages 4 and 5 vertical velocity do however not depend on light ($w_{Li} = 0$).

The vertical velocity in response to pH for stages -1 to -3 was obtained by doing a linear regression based on Gravinese et al. (2018) data:

$$w_{pH} = (-14.64 + 1.846 \cdot pH)/100$$

Based on Gravinese (2018)'s observations, we finally defined a stage-specific damping factor $\alpha_{p,i}$ that reduces the vertical velocity in response to pressure changes:

$$\alpha_{p,i} = \begin{cases} \dfrac{1}{2 + exp\left(10^5 \cdot \left(\mathrm{w_L} + \mathrm{w_{pH}} - 0.0005\right)\right)} + 0.5 & , i = 1 \\ -exp\left(-\dfrac{\left(\mathrm{w_L} + \mathrm{w_{pH}} + 0.0016\right)^2}{2 \cdot 0.0005^2}\right) + 1 & , 2 \leq i \leq 3 \\ -1.18 \cdot \left|sin\left(\dfrac{\pi}{0.2776 \cdot 3600} \cdot t\right)\right| + 1 & , 4 \leq i \leq 5 \end{cases} \quad (12)$$